Phonon-Induced Desorption of Adatoms from Crystal Surfaces. II. Numerical Computations for a Model System*

See-Chen Ying†
Department of Physics, Brown University, Providence, Rhode Island 02912
and
Bernard Bendow
Solid State Sciences Laboratory, Air Force Cambridge Research Laboratories, Bedford, Massachusetts 01730
(Received 24 May 1972)

The energy and angular distributions of desorbed adatoms, and the temperature dependence and absolute magnitude of the desorption rate, are studied numerically within a three-dimensional quantum treatment of desorption. Model parameters appropriate to Ne adsorbed on Xe-covered graphite are employed. The angular distribution is found to peak strongly in the forward direction, and the energy distribution peaks strongly for final adatom energies near to zero. The temperature dependence of the rate is found to vary as $e^{-\beta E_0}$, with a prefactor $\sim 10^5$ sec^{-1}.

I. INTRODUCTION

The desorption of adatoms from solid surfaces has long been a subject of considerable interest, both theoretically and experimentally.[1] In the preceding paper (henceforth referred to as I), we presented a three-dimensional multiphonon-quantum theory of phonon-induced desorption. The results of the formal theory were applied to obtain various expressions for the desorption rate of adatoms from localized states, for systems characterized by a Morse-like interaction potential between the adatom and the crystal atoms, and for a bulk Debye model of the substrate.

In this paper we present various numerical computations of the single-phonon rate as derived in Sec. IV of I. A numerical computation of the multiphonon rate, including up to three-phonon processes, based on the multiphonon expression given in Eqs. (4.20) and (4.23) of I, was presented in Ref. 2. The essential features of the latter computations are summarized in Sec. II. The principal quantities of interest in the present paper are the energy and angular distributions of desorbed adatoms, and the temperature dependence and absolute magnitude of the desorption rate. The dependence of the rate on various system parameters and on the substrate structure is also considered. For simplicity, we here employ just the bulk-mode correlation function appropriate to a free surface, C_B (see Sec. IV of I). The extension to include surface modes involves a straightforward, although more tedious, computation which we do not undertake here.

In Sec. II we describe computations for model parameters appropriate to Ne adsorbed on Xe-covered graphite,[3,4] and present the results. In Sec. III we summarize our conclusions, and make contact with predictions based on the formal results of the preceding paper. A comparison with other theories and a discussion of the relation to experiment are also given.

The notation employed here is that of the preceding paper, to which the reader should refer for the detailed meanings of various symbols.

II. NUMERICAL COMPUTATIONS FOR MODEL SYSTEM

A. Description of Computations

In this section we present a description of the computation of the single-phonon rate as derived in Paper I. The rate takes the form

$$R(\vec{k},\theta)=2\pi R_0^{(1)}\sum_{i,X_{ij},z_i,z_j,\pm} f_1^i(\pm,lj,\beta,E)$$
$$\times[J_0(d_2^iX_{ij}k\sin\theta)\,(a_0^i+a_1^i\tilde{k}_z+a_3^ik^2\sin^2\theta+a_4^i\tilde{k}_z^2)$$
$$-a_2^iX_{ij}\,k\sin\theta\,J_1(d_2^iX_{ij}\,k\sin\theta)]$$
$$\times\exp(d_0^i+d_1^i\tilde{k}_z+d_3^ik^2\sin^2\theta+d_4^i\tilde{k}_z^2)\,, \quad (2.1)$$

where

$$f_1^i\equiv\sin[k_0\gamma_{ij}^{\pm}E(\vec{k})]\,(\gamma_{ij}^{\pm})^{-1}(e^{\beta E(\vec{k})}-1)^{-1}$$
$$\times\frac{\{E_z(\vec{k})/[\bar{E}_0+E_z(\vec{k})]\}^{1/2}s_0^i}{s_3^i(s_1^is_2^i)^{1/2}}\,,$$
$$R_0^{(1)}\equiv\tfrac{1}{16}\pi\omega_D\gamma_4^2h_0^2k_0^{-1}\,,$$
$$h_0^2\equiv 2^{11}(\tfrac{1}{2}\pi)^{1/2}\pi^4\tilde{V}_0^2\gamma_1^6\gamma_2^2\gamma_3e^{r_0^2/2r_1^2}\,,$$
$$\tilde{k}_z^2\equiv 2m_a\bar{E}_0+k^2\cos^2\theta\,,$$
$$\gamma_{ij}^{\pm}\equiv[X_{ij}^2+(z_i\pm z_j)^2]^{1/2}\,,$$

where k is the final adatom momentum, θ is the desorption angle (measured from the normal to the surface), the J's are Bessel functions, and $R_0^{(1)}$, s^i, and the a_i's and d_i's, are defined in detail in Sec. V of I. The latter are functions of the fundamental parameters r_i^2, m_i, and E_0. r_0 and r_1 are the parameters of the interatomic Morse-

like model potential v, where $v = \tilde{V}_0(f^2 - f)$, $f \equiv \exp[-\frac{1}{8}(r^2 - r_0^2)/r_1^2]$; r_2 and r_3 are the vibrational ranges in the localized initial-state wave function $\psi \sim \exp[-\frac{1}{4}(x^2+y^2)/r_2^2 + (z-z_0)^2/r_3^2]$; m_a and m_s are the adatom and substrate masses, respectively; E_0 is the "binding energy" of the adatom in its well; $\bar{E}_0 \equiv E_0 - U_0 + \epsilon_0$, where $2U_0$ is the lateral variation in the adatom potential $V^0(\vec{r})$ and ϵ_0 is the energy of the adatom measured from the well bottom (see Fig. 2 of I); and $c_0 = \hbar^2/m_s\omega_D a_0^2$ is the multiphonon expansion parameter.

In a first-principles formulation, the specification of $v(\vec{r})$, and the substrate configuration, enables one to compute $V^0(\vec{r})$. Averaging V^0 over all angles in the surface plane, one may then obtain r_2 and r_3 as ($\hbar = 1$)

$$r_2^2 = \tfrac{1}{2} m_a^{-1} \left(\frac{\partial^2 V^0}{\partial \vec{X}^2}\right)_0^{-1}, \quad r_3^2 = \tfrac{1}{2} m_a^{-1} \left(\frac{\partial^2 V^0}{\partial z^2}\right)_0^{-1}, \qquad (2.2)$$

where 0 indicates evaluation at the well minimum. Likewise, E_0, $\bar{E}_0$, and z_0 follow directly once V^0 has been averaged over the plane. These parameters (plus those specifying v) determine fully the adatom properties. In practice, the above procedure is limited by the availability of systems for which the full complement of substrate and adatom microscopic properties are known.

For the present computations we employ the results of a computation of V^0 for Ne adsorbed on Xe-covered graphite (carbon black), as carried out by Steele *et al.*[3,4] This seems to be one of the few physisorption systems where detailed computations of V^0, and comparison with experiment, has been pursued. However, the main intent of the present computations is not to obtain quantitatively accurate predictions for the particular system Ne-Xe-C. Rather, we employ the available data for this system as a basis for choosing qualitatively reasonable parameters with which to pursue representative computations for low-temperature physisorption systems.

Values of certain of the parameters employed are listed in Table I. Some of the choices of the parameters in the computations involve the following considerations.

(a) Compromises between theoretically predicted and experimentally observed values were made when these were in conflict.

(b) Although the model employed in obtaining V^0 is the Lennard-Jones potential v_{LJ}, we employ the Morse-like potential v in computing the interaction matrix elements. In most of the computations, we employ for the additional range parameter r_1 in v the value unity, although the hard core disappears for this value. The presence of the hard core should be less important for the present model, where the assumptions of a highly localized initial state, and deep well for the final state, are built into the model. In support of the latter contention, we will indeed find that the rate varies comparatively slowly with r_1, as r_1 is varied from unity down to values where v closely simulates v_{LJ} (see Paper I). In a more detailed treatment, one may consider two other possible criteria: the shape of the total V^0 arising from v's with various r_1's, as compared to that resulting from v_{LJ}; and the values of the curvatures at well bottom for v as opposed to v_{LJ}. As these various criteria generally lead to different values of r_1, the use of v would appear to be most reliable when the dependence of R on r_1 is weakest.

TABLE I. Ne-Xe-C parameters.

Xe substrate structure: simple cubic.
Xe lattice constant $a_0 = 4.31$ Å.
Adatom vibrational energy $\nu = 56$ °K.
Vibrational range in plane, $r_2/a_0 = 6.2 \times 10^{-2}$.
Vibrational range in z, $r_3/a_0 = 2.8 \times 10^{-2}$.
Adsorption distance $z_0/a_0 = 1$.
Bulk-mode Debye temperature $T_D = 343$ °K.
Phonon expansion parameter $C_0 = 0.85 \times 10^{-4}$.
Well depth energy $E_0 = 231$ °K.
Potential variation in plane $2U_0 = 100$ °K.

(c) The numerical results displayed in Ref. (3) are not detailed enough to compute r_2 and r_3 accurately. Rather we assume that the localization of the adatom is greater in the z direction relative to that in the plane. Correspondingly, we choose to break up the available value of the adsorbed state vibrational energy in the arbitrary proportion of 5 : 2 in the z relative to the plane.

(d) The phonon model ought to include modes appropriate for a coupled Xe-C substrate. Information about these modes does not seem to be available, but even if it were, it is unlikely that the details could be adequately incorporated in a simplified Debye model such as employed here. For these reasons, we adopt the view that a small number of Xe layers do not significantly affect the bulk-mode correlation function C_B, so that a Debye model for the graphite alone is appropriate.

As noted previously, the computation of the rate involves a sum over discrete sites, which accounts for the particular geometry of the substrate in the vicinity of the adatom. The number of sites necessary in the sum depends on the system parameters, as may be observed directly from Eq. (2.1). For the Ne-Xe-C system, it was found that to obtain R to an accuracy of about 5%, one needs to include sites such that $r_\pm^2 \equiv \vec{X}_{lj}^2 + (z_l \pm z_j)^2 \approx 30$–$40$. In general, this necessitates including about twenty distinct (nonequivalent) sites in the plane. One reason why so many sites need to be considered, despite the exponentially decreasing behavior evident from Eq. (2.1), is that the con-

tributions from each site oscillate in sign, as may be seen from the $\sin(r_{\pm}\cdots)$ factors. The computations presented here carry out the sum over sufficient sites so as to achieve about 5% accuracy. Examples of the site configurations for various cases are illustrated in Fig. 1.

In the present computations of the rate, we do not include the rapidly oscillating contributions of Paper I, as these lead, in general, to a small contribution to the total rate, and because such oscillations are expected to be difficult to observe experimentally. To obtain an estimate of the oscillation involved, let us consider the behavior for a square well of width $(z_0 - a)$. The factor e^{2iFa} appearing in Eq. (4.17) of I for the rate then becomes $e^{2i\tilde{k}_z a + \pi/4}$. For $E(k) \ll E_0$, where the rate is largest, $\tilde{k}_z \approx (2m_a E_0)^{1/2}\,[1 + 0.5E(k)/E_0]$. For example, for $E_0 \sim 0.5$, $a \sim a_0 \sim 1$, one has an oscillatory factor $\sim \exp[2i\sqrt{m_a}E(k)]$; for Ne, $\sqrt{m_a} \sim 60$ in dimensionless units, corresponding to a period ~ 20 oscillations per unit energy; for an m_a appropriate to xenon the period ~ 50. In a more detailed treatment, or when greater accuracy is required, it is straightforward to include these terms in numerical computations in an exactly parallel fashion to the nonoscillatory terms computed here.

Comparison with bulk computations. As demonstrated in the present treatment, various differences arise between the calculation of rates at surfaces of solids, as opposed to those in the bulk. These stem principally from the breaking of the translational invariance at the crystal surface. For example, while only single sums over q_z and z_{lj} would result in the bulk case, double sums, over q_z and q_z', and z_l and z_j, remain in the surface case. In constructing the correlation function C, boundary conditions at the surface need be accounted for. A calculational aspect peculiar to problems such as desorption is the necessity for summing over a discrete configuration of lattice sites $\vec{R}_l$ in computing R, instead of integrating over $\vec{R}_l$. The influence of the specific nature of the lattice configuration in surface problems is well known in a wide variety of situations. More than merely a single or few sites are required in computing R, in general, although the sum does converge rapidly when $|\vec{R}_l|$ exceeds some finite value.

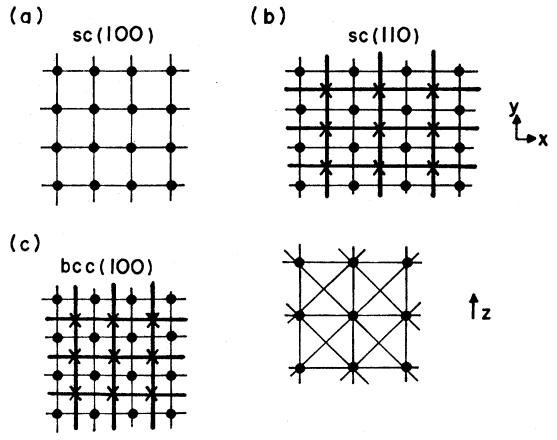

FIG. 1. Geometrical configurations describing sc (100), sc (110), and bcc (100) adsorption. (a) xy, yz, and xz planes of sc (100). (b) sc (110) configuration. (c) The same for bcc, indicating the alternating layers of atoms comprising unit cells.

The sum over sites and the time Fourier transform can be carried out analytically for the Einstein model. The former is a consquence of δ functions in $(\vec{R}_l \pm \vec{R}_j)$ arising in C. The latter follows by equating transforms of the form $\int dt \exp(i\omega t + ae^{\pm i\omega_0 t})$ to sums over Bessel functions. The computational advantages of this model, however, are offset by its artificiality. For this reason, we have not here presented computations within the Einstein model. In connection with problems where the optical modes dominate the processes of interest, such as may be the case in photodesorption, for example, computations within the Einstein model may become appropriate.

B. Results

In this section computations of the single-phonon rate of Eq. (2.1), illustrating various dependences, are presented.

Figure 2 illustrates the rate $R(k, \theta = 0)$ (which is the desorption rate per unit solid angle in the forward direction, integrated over all angles in the plane) as a function of the adatom's final energy $E = k^2/2m_a$, for Ne-Xe-C. The effect of variations in r_0, r_1, r_2^2, and r_3^2, E_0, and m_a, are also illustrated. The curves are truncated at the single-phonon cutoff appropriate to the two values of E_0 employed [for the energies above the cutoff Eq. (2.1) is, of course, not applicable]. A general feature of the results is the strong peak near $E = 0$, corresponding to an extremely narrow energy distribution of desorbed adatoms. For energies above the peak, R is seen to be very nearly an exponentially decreasing function of E. The fact that R peaks at a value of E somewhat above $E = 0$ is a consequence of the WKB wave function, which is proportional to $\sqrt{E}$; for a free final state, for example, the peak would occur exactly at $E = 0$.

Figure 3 illustrates the rate for desorption in the forward direction, $R(\theta = 0)$, as a function of temperature. R is seen to follow a nearly exponential law, $R \cong R_0 \exp(-\beta E_0')$, at low temperatures, departing somewhat at higher temperatures, where Bose–Einstein statistics become important. Note that the effective adsorption energy E_0' exceeds E_0, being close in value to the energy for which

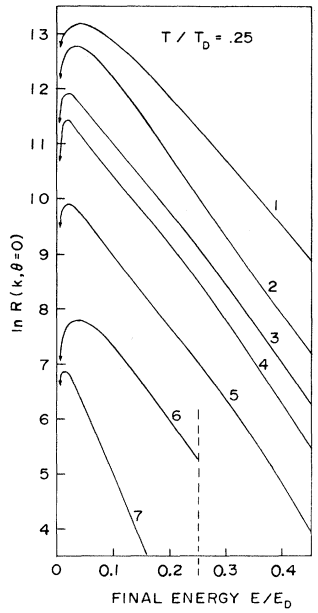

FIG. 2. ln of desorption rate in normal direction $R(k,\ \theta=0)$ vs final energy E/E_D. All curves are for parameters listed in Table I with the following variations: (1) $r_1=0.25$; (2) $r_1=0.5$; (3) no variation; (4) $r_0=0.75$, $z_0=0.75$; (5) $r_2^2\rightarrow 2r_2^2$; (6) $E_0=0.75$; (7) $m\rightarrow 2m$. Calculations are carried out for $T/T_D=0.25$. See, also, the footnote to Table II.

the product $E(k)R(k)$ is maximal. For Ne-Xe-C the prefactor $R_0\sim 10^5$ sec^{-1}. Values of R_0 and $\tau_0\equiv R_0^{-1}$ corresponding to various values of the parameters are listed in Table II.

Figure 4 illustrates the angular properties of desorbed adatoms. Figure 4(a) shows that rate $R(\theta)$ peaks strongly in the normal direction compared to the $\cos\theta$ distribution. Increasing θ is also associated with a sharper peak in the energy distribution, as illustrated in Fig. 4(b). Temperature dependences are illustrated in Fig. 4(c). As the peaks in Fig. 3(b) occur at nearly the same E, the R vs T^{-1} curves are nearly parallel. The total rate for the parameters of Fig. 4 is approximately $0.8R(\theta=0)$ at 25 °K, corresponding to a prefactor $\sim R_0$, the prefactor obtained from the $R(\theta=0)$ rate. The value of R_0 is seen to be considerably smaller than the adatom vibrational period $\nu^{-1}\approx 10^{12}$.

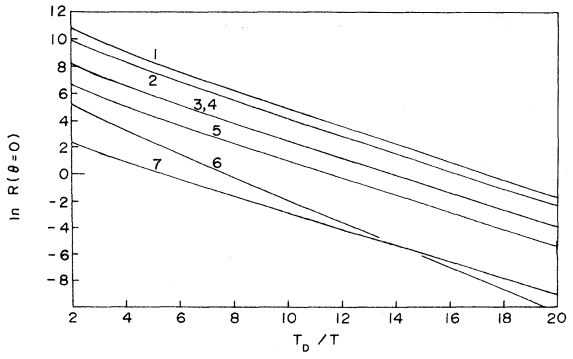

FIG. 3. ln of total rate in forward direction, $R(\theta=0)$ vs inverse temperature T_D/T. Labels correspond to those in Fig. 2.

TABLE II. Desorption rate prefactors, and lifetimes at $T=0.25T_D$.

Case	R_0(sec^{-1})	τ_0(sec)	$\tau[T/T_D=0.25]$(sec)
$r_1=0.25$	8.1×10^5	1.2×10^{-6}	7.2×10^{-4}
$r_1=0.50$	3.3×10^5	3.0×10^{-6}	1.8×10^{-3}
$r_1=1.0$	7.3×10^4	1.4×10^{-5}	8.4×10^{-3}
$r_2^2=2r_2^2$	1.6×10^4	8.6×10^{-5}	5.2×10^{-2}
$m_a\rightarrow 2m_a$ [a] $m_s\rightarrow 2m_s$	3.0×10^1	3.3×10^{-2}	2.0×10^1
$E_0\rightarrow 0.75$	5.5×10^2	1.8×10^{-3}	7.2
bcc(100)	6.0×10^4	1.7×10^{-5}	1.0×10^{-3}

[a]Note that variations in m alone are not, strictly speaking, physically reasonable. Since $r_{2,3}^2\propto m_a^{-1}$ [cf. Eq. (2.2)] and since it is the combination $r_{2,3}^2 m_a$ that appears in the crucial places in the rate, it is more appropriate to view the present results as approximately appropriate to variations in the product $m_a r_{2,3}^2$.

The dependence of desorption on the substrate structure is considered in Fig. 5, where the rate for sc (100), sc (110), and bcc (100) faces is illustrated (see also Fig. 1). The magnitude and shape of the energy distribution is seen to indeed depend on the substrate configuration, as would be expected. For example, a difference of about a factor of 3 between the value of R_0 for sc (100) and sc (110) is predicted. Differences in the energy distribution are washed out in the temperature dependence, as illustrated in Fig. 5(b).

Note that in our derivation of the desorption rate of Sec. II A, we have suppressed various factors of volume and area for notational convenience. A careful accounting of these factors shows that the desorption rate is proportional to the factor a_0^2/a_s, where a_s is the surface area per substrate atom. In addition, the function C is proportional to v_0/a_0^3, where v_0 is the volume per particle; also $a_0^3 k_D=6\pi^2 a_0^3/v_0$. For the sc structure $a_0^2/a_s=v_0/a_0^3=1$, leading to the results in Sec. II A. To compare bcc results to sc, we choose in the bcc case to scale by $0.8a_0$ (rather than a_0), which is very close to the interatom separation, but leaves k_0 unchanged. Thus $r_1^2\rightarrow 0.64r_1^2$, for example.

The effect of employing a smaller number of sites in the sum in computing $R(k)$ is illustrated in Fig. 5(a). Oscillations that result in this instance are smoothed out as more and more sites are included.

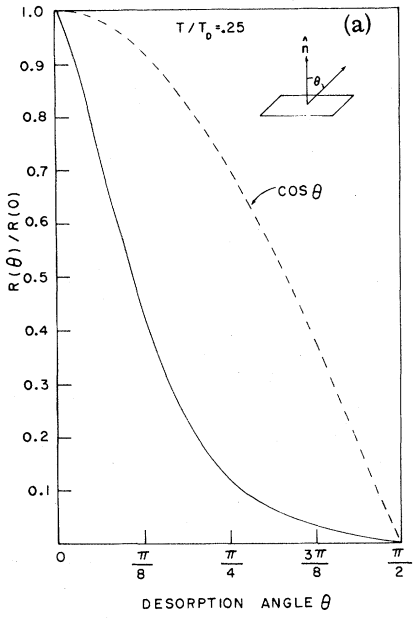

FIG. 4. Angular properties of the desorption rate. (a) $R(\theta)/R(0)$ vs desorption angle θ, for Table I parameters, at $T/T_D = 0.25$. (b) Energy distributions, in $R(k, \theta)$ vs $E(k)/E_D$, at different desorption angles. (c) Total rate vs T_D/T at different angles.

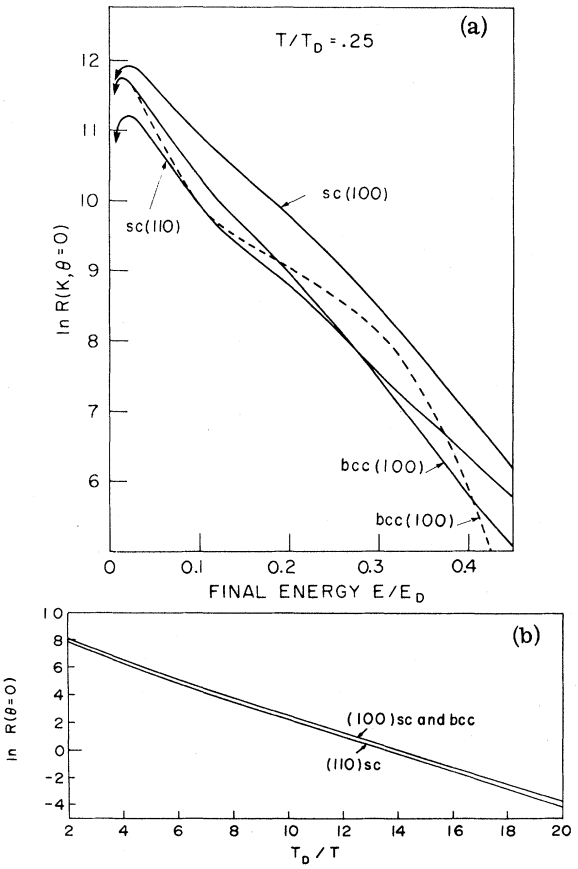

FIG. 5. Effect of substrate configuration on desorption rate. (a) ln $R(k, \theta = 0)$ vs E/E_D for three configurations. The dotted line indicates results of the bcc (100) computation when the number of sites included is half that in the solid-line curve. (b) ln$R(\theta = 0)$ vs T_D/T for various configurations.

To obtain a picture of the multiphonon properties of the rate, we refer to the computations in Ref. (2). These results indicate[5] that at the nth phonon cutoff, the energy distribution suffers an abrupt decrease of order C_0, as expected from I. These discontinuous drops in R reflect the abrupt cutoff characterizing the Debye spectrum. For a more realistic phonon spectrum, the decrease would be expected to become continuous. It is clear from these observations that at low temperatures the lowest phonon process allowed by energy conservation dominates the rate.[6] The multiphonon formalism is most useful when only higher-order phonon processes are allowed because of energy conservation, or for high-temperature computations (not considered here) where the phonon population is proportional to T.

III. DISCUSSION

In this section we summarize the general properties of the desorption rate emerging from the

present treatment and discuss the sensitivity on various system parameters. Comparison with one-dimensional surface calculations and a discussion of the relation between theory and experiment is given.

A. General Properties of Desorption Rate

We briefly outline various general properties of the desorption rate emerging from the analytical and computed results of the present treatment.

At very low temperatures, the dependence of $R(k)$ and R on β is very nearly $e^{-\beta E}$, where $E = E(k)$ for $R(k)$ and $E = E_0' \gtrsim E_0$ for R. The effective adsorption energy E_0' exceeds the well depth E_0, as discussed in Sec. II B. At higher T, the Bose–Einstein statistics describing the phonons lead to deviation from the exponential law.

The energy distribution of desorbed atoms peaks sharply at a value of final adatom energy E near zero. The peak lies above, rather than at, zero because of the proportionality of the distorted final-state wave function to $\sqrt{E}$. The rate decreases nearly exponentially above the peak, as a result of exponentially decreasing terms arising in the factor $\phi(\vec{k} - \vec{q})$ entering the transition matrix element. Also, as the energy increases to where n phonons are required to conserve energy, the rate decreases by C_0^{n-1}. The decrease occurs abruptly for the Debye model at each n-phonon cutoff, but smooths out for more realistic phonon spectra.

The total rate is characterized by prefactors[7] many orders of magnitude smaller than the vibrational frequency of the adatom in its well, as opposed to the classical theory of Frenkel.[8] The prefactor R_0 is found to be typically $\sim 10^5$ sec^{-1} for the Ne-Xe-C system. This result is consistent with perturbation theory, which requires that $R_0 \ll$ adsorption binding energy.

The angular distribution peaks very sharply in the forward direction as compared to a $\cos\theta$ distribution. The total rate over all desorption angles θ turns out to be of the same order of the differential rate with respect to $\cos\theta$. To compute the angular distribution more accurately, diffraction effects need to be included in computing $\phi(\vec{k})$, and the Umklapp terms included in obtaining $R(\theta)$.

B. Sensitivity of Rate on System Parameters

From Paper I one observes that the rate depends via exponential factors on the binding energy E_0, and the ranges r_i. For typical values of the remaining parameters, the sensitivity on r_2^2 and r_3^2, through d_3^i and d_4^i of Eq. (2.1), for example, is the strongest from among the r_i's. Typically $r_0 \sim 1$ for physisorption systems, and the dependence on r_1 is relatively weak. The strong dependence on r_2^2 and r_3^2 may result in strong angular variations in desorption, and departures from $\cos\theta$ distributions such as illustrated in Fig. 4(a). For $r_2^2 > r_3^2$, as is generally the case, the distribution peaks strongly in the forward direction. In order to obtain accurate theoretical predictions of the magnitude, and energy and angular dependence of the rate, one thus requires accurate input values for r_2^2 and r_3^2.

One may deduce from Eq. (2.1) that in general one must sum over an extended number of sites to obtain accurate results for R. The shape of the energy distribution, for example, is extremely sensitive to the number of sites included, as mentioned in Sec. II. The present results demonstrate clearly the inadequacy of the approach of Lennard-Jones, Devonshire, and Strachan (LJDS),[9] where only a single site is included in the sum.

A strong dependence of the rate on the adatom mass is also evident, the rate decreasing rapidly with increasing m_a and all other parameters remaining fixed. However, it is clear that a change in m_a strongly influences the r_i's and E_0, so that considering changes in m_a alone may not be meaningful.

As demonstrated in Sec. II, the rate does depend on the substrate configuration, although relatively weakly. This result is anticipated by noting the oscillatory nature of the contributions by site to the rate, which minimizes the effect of the detailed distribution of the sites in the vicinity of the adatom. In the present treatment, the desorption rate depends only on the adsorption energy E_0, but is independent of adsorption position above the substrate cell (see Sec. III of I).

As mentioned above in various connections, detailed dependences on system parameters involve the strong interdependence of the various parameters. For example, it is only partly meaningful to characterize the dependence of R on v_0 as proportional to v_0^2, since v_0 affects the size of V^0 and thus r_2^2, r_3^2, and E_0. These observations point out the desirability for self-consistent computations following from a single microscopic model, although such a computation is a formidable task. Alternatively, one must rely on consistent experimental values for the parameters.

C. Differences between One and Three Dimensions

Goodman[10] has remarked that one-dimensional treatments of desorption yield abnormally large rates because all energy transfers necessarily lead to motion normal to the surface, while in the three-dimensional case, motion in the surface plane supplies an alternate sink to the energy transfer. Two reasons for the smaller rate that emerge clearly from the present treatment are the following.

(a) The three-dimensional density of adatom

states, which leads to $\int dk\, k^2$ integrals in place of the one-dimensional $\int dk$. Since the differential rate is strongly peaked about $k \sim 0$, the total rate is substantially decreased through the density of states in the three-dimensional case.

(b) The well depth V_m^0 is much larger in the three-dimensional case than in the one dimensional, generally by about a factor of 3–10, depending on the geometrical configuration.[11] The transition rate, however, is still proportional to only v, as evidenced by the oscillation in sign of the contributions to the rate in the sum over sites. Since the rate decreases rapidly with increasing E_0, the decrease in the ratio of v/V_m^0 for the three-dimensional case thus leads to a sharply diminished desorption rate.

Inspection of Strachan's work,[6] where only motion perpendicular to the surface was considered, also yields rates much smaller than the Frenkel theory. A strict comparison with the present theory is difficult, but it appears that the present approach does yield rates smaller than the LJDS theory.

D. Effects of Realistic Phonon Spectra

In Paper I various limitations of the present model for real surfaces were noted. It was also pointed out that the details of energy and angular distributions are expected to depend on the details of the phonon spectrum. We here emphasize that a quantitatively accurate calculation of desorption must account properly for surface modes. The frequency distribution for various surface lattice models can be, in fact, similar to the Debye case (cf. Figs. 5 and 6 of Ref. 12, for example). In general, of course, the distribution is characterized by a variety of peaks, as demonstrated in, e.g., Ref. 13. The distribution is also affected in various ways by the presence of an absorbed layer.[13]

In principle, the contributions of surface and bulk modes to desorption are of the same order of magnitude. Roughly speaking, each of the N atoms in the bulk contributes $1/N$ to the mean-square amplitude $\langle u_l^2 \rangle$ of a surface atom, and each of the N_s surface atoms contributes $1/N_s$. It is well known that $\langle u_l^2 \rangle$ for surface atoms is generally several times larger than that for the bulk atoms.[14] The present model may easily be seen to follow an analogous behavior, as a result of the boundary conditions employed in computing C. Thus bulk modes do account qualitatively for various aspects of observed surface properties, although the contribution of surface modes, being of the same order of magnitude, needs to be included for quantitatively accurate results. We also note that the contribution of surface modes to desorption depends on the system energetics. Since the frequency distribution of the surface modes generally peaks at lower frequencies, whenever E_0 exceeds the peak frequency, it is only the bulk modes that contribute in lowest order to the rate. For the parameters employed in Sec. II A, for example, this is, in fact, most probably the case.

E. Relation to Experiment

We discuss briefly some possible experiments to measure desorption lifetimes and velocity distributions. A detailed review of applicable experimental techniques may be found in Ref. (15), for example.

One type of relevant experiment is the scattering of molecular beams from solid surfaces.[1,16] A pulse of molecules that are collimated and frequency modulated to produce a beam is scattered from a surface, and the energy, angular distribution, and phase of the reflected molecules measured. Those molecules that are adsorbed and thermalized will desorb with incoherent phase, and with a different angular distribution from the directly scattered molecules. Thus, the desorption spectrum should be distinguishable from the direct scattering. So far it appears that such experiments have only been carried out for chemisorption systems, such as[16] H_2 beams on Ni, for example. Similar experiments for physisorbtion systems would necessitate low temperatures, conditions under which it is difficult to obtain clean surfaces. However, scattering from contaminated surfaces can still be of interest and amenable to theoretical interpretation as long as the impurity layer is ordered or partially ordered—such as is the case with an epitaxial layer of oxygen.

A second type of experiment relating to measurement of τ_0 is the time-of-flight method. Recently, Pollock *et al.*[17] measured the diffusion time for helium propagating down a Cu capillary tube. The time of flight is related to the mean free path of He, the sticking probability ξ of He on Cu, and the mean residence time on the tube walls. A relation obtained by the authors of Ref. (16) is

$$\xi\tau = (2\pi)^2 (\hbar^3/m_a)\bar{\nu}\beta^2 e^{-\beta E_0}, \tag{3.1}$$

where $\bar{\nu}$ is the number of adsorption sites per unit area. Applying this relation to the results of the present paper, where $\tau_0 \sim 10^{-5}$ sec, yields an estimate for $\xi \sim 10^{-5}$–10^{-6}. Since experimental data applicable to the present case are not available, there is no way of gauging the correctness of this estimate. On the other hand, the classical-theory estimate, which would yield $\tau_0 \sim 10^{-13}$, leads to the absurd result that ξ, which must lie between zero and unity, is much greater than unity.

It is hoped that experiments of the variety discussed here will be carried out in the near future,

so as to enable an extensive comparison between theory and experiment for low-temperature desorption.

ACKNOWLEDGMENTS

The authors thank John Beeby, Walter Kohn, Herb Shore, and Harry Suhl for useful discussions.

*Part of this work was carried out while the authors were at the Department of Physics of the University of California, San Diego. The support of ONR and NSF (S.Y. and B.B.) and AFOSR (B.B.) during this time are acknowledged.

†A. P. Sloan Research Fellow.

[1] See, for example, *The Structure and Chemistry of Solid Surfaces*, edited by G. A. Somorjai (Wiley, New York, 1969); *The Solid-Gas Interface*, edited by E. A. Flood (Marcel Dekker, New York, 1967); and *Fundamentals of Gas-Surface Interactions*, edited by H. Saltsburg *et al.* (Academic, New York, 1967).

[2] S. C. Ying and B. Bendow, Phys. Lett. A 37, 91 (1971); B. Bendow and S. C. Ying, J. Vac. Sci. Technol. **9**, 804 (1972).

[3] W. A. Steele and M. Ross, J. Chem. Phys. 35, 850 (1961).

[4] M. W. Barnes and W. A. Steele, in *Fundamentals of Gas-Surface Interactions*, Ref. 1.

[5] The results of Ref. 2 represented preliminary computations where only a limited number of sites were used in the sum over sites. For this reason, the single-phonon spectrum shown there revealed an oscillatory behavior, which is smoothed out when sufficient sites are included in the sum, as discussed in the present paper.

[6] A similar conclusion was reached by C. Strachan, Proc. R. Soc. A **150**, 456 (1935).

[7] The general range of experimentally observed τ's is discussed, e.g., by L. A. Petermann, Nuovo Cimento Suppl. **5**, 364 (1967), and references therein.

[8] See, for example, J. Frenkel, Z. Phys. **51**, 232 (1928).

[9] J. E. Lennard-Jones and C. Strachan, Proc. R. Soc. A **150**, 442 (1935); C. Strachan, Ref. 6; J. E. Lennard-Jones and A. F. Devonshire, Proc. R. Soc. A **156**, 6 (1936); Proc. R. Soc. A **156**, 29 (1936).

[10] F. Goodman, Surf. Sci. **24**, 667 (1971).

[11] R. J. Bacigalupi and H. E. Neustadter, Surf. Sci. **19**, 396 (1970).

[12] R. E. Allen and F. W. de Wette, J. Chem. Phys. **51**, 4820 (1969).

[13] R. E. Allen, G. P. Allredge, and F. W. de Wette, Phys. Rev. B **4**, 1648 (1971); Phys. Rev. B **4**, 1661 (1971); Phys. Rev. B **4**, 1682 (1971).

[14] C. B. Duke, Ann. Rev. Mater. Sci. **1**, 165 (1971) and references therein.

[15] J. DeBoer, *Dynamical Characters of Adsorption* (North-Holland, Amsterdam, 1969).

[16] See, for example, R. L. Palmer *et al.*, J. Chem. Phys. **53**, 1666 (1970); and S. Yamomoto and R. E. Stickney, J. Chem. Phys. **47**, 1091 (1967).

[17] F. Pollock, H. Logan, J. Hobgood, and J. G. Daunt, Phys. Rev. Lett. **28**, 346 (1972).

PHYSICAL REVIEW B VOLUME 7, NUMBER 2 15 JANUARY 1973

Lattice Dynamics, Third-Order Elastic Constants, and Thermal Expansion of Titanium

R. Ramji Rao and C. S. Menon*

Department of Physics, Indian Institute of Technology, Madras-36, India

(Received 22 February 1972)

The lattice dynamics, second- and third-order elastic constants, and the anisotropic thermal expansion of hexagonal titanium are worked out using Keating's approach. The ten third-order elastic constants are calculated using five third-order parameters. The experimental measurements on the pressure derivatives of the second-order elastic constants in titanium are in good agreement with the calculated values. The low- and high-temperature limits $\bar{\gamma}_L$ and $\bar{\gamma}_H$ of the lattice thermal expansion are calculated and compared with those obtained from the thermal-expansion data of titanium. The lattice dynamics of titanium is found to be similar to that of zirconium.

I. INTRODUCTION

Titanium crystallizes in a hexagonal close-packed structure at atmospheric pressure and low temperatures with $c/a = 1.5884$. Titanium and zirconium belong to group IV A and are exceptionally similar in many physical and chemical properties, and both of them undergo phase transformations to the bcc structure at high temperatures. Experimental dispersion relations in titanium are not available in the literature. The second-order elastic constants of titanium were experimentally determined by Fisher and Renken[1] and their pressure derivatives were recently reported by Fisher and Manghnani.[2] Using Keating's approach,[3] the lattice dynamics and the expressions for the second-order elastic (SOE) and third-order elastic (TOE) constants of the hexagonal metals have been worked out by Srinivasan and Rao[4,5] and used successfully to investigate the anharmonic properties and anisotropic thermal expansion of magnesium, zinc, and beryllium.[4,5] In this paper the lattice dynamics, SOE and TOE constants, and temperature variation of the lattice thermal expansion of hexagonal titanium have been calculated.

II. POTENTIAL ENERGY IN KEATING'S APPROACH

The basis vectors of the lattice are $\vec{a}_1 = D(\frac{1}{2}\sqrt{3}, \frac{1}{2}, 0)$, $\vec{a}_2 = D(0, 1, 0)$, and $\vec{a}_3 = D(0, 0, p)$, referred to the Cartesian system of axes. Here $D = a$ is the